J Therm Anal Calorim (2013) 111:1255–1262
DOI 10.1007/s10973-012-2369-4

Thermal study of a shape memory alloy (SMA) spring actuator designed to insure the motion of a barrier structure

Sonia Degeratu · P. Rotaru · S. Rizescu · N. G. Bîzdoacă

CEEC-TAC1 Conference Special Issue

Abstract The study concerns an experimental model using a SMA spring actuator for improving the whole performance of a barrier structure. The study is, specifically, focused on the thermal analysis of the SMA spring material and on determination of the SMA spring working time periods at different values of the activating electric current inducing different phase changing speeds.

Keywords Barrier structure · SMA spring · Thermal analysis · Mathematical model

Introduction

The barrier structures' performances are directly related to the actuators' driving systems' performance.

This paper presents a study that was made on a barrier structure experimental model, conceived by the authors and powered by a shape memory alloy (SMA) spring based actuator. Here, the SMA spring works as an actuator by contracting with great strength and speed, and exerting the necessary force to lift the barrier arm when heated.

The authors have chosen an actuator of this kind because, unlike any traditional actuator, it needs no lubrication, is silent, environmental friendly while having a small number of moving parts. Moreover, an actuator like this one can be miniaturized and allows full control on its functioning regime(s) [1–5]. All these advantages are deriving from the SMA's unique properties, specifically from the *Shape Memory Effect (SME).*

SMA is able to memorize and recover its original shape, after it was deformed, by heating beyond its transformation temperature. This unique effect of returning to its initial geometry after a large inelastic deformation is known as the SME [2, 6–8]. The SME occurs due to martensitic phase transformation, between a low temperature phase, called martensite (M), and a high temperature parent phase, called austenite (A). A typical shape memory element has four relevant temperatures that define the different stages of actuation, thus providing the designer a method for control. Simply, the four temperatures define the start and finish transformations for martensite (M_s, M_f) and austenite (A_s, A_f).

The process of returning to the initially memorized form was put in evidence for the first time in 1932, by Arne Olander, in case of some gold (Au)- and cadmium (Cd)-based alloy. In 1958, researchers Chang and Read demonstrated the shape memory effect at the Brussels World's Fair. Specifically, they showed that the SME could be used to perform mechanical work by cyclically lifting a weight using an Au–Cd SMA [2, 3, 8].

In 1961, a group of U.S. Naval Ordnance Laboratory researchers led by William Beuhler, discovered an alloy of nickel and titanium, exhibiting the SME. Then, researchers,

S. Degeratu
Department of Electromechanics, Faculty of Electrical Engineering, Environment and Industrial Informatics Engineering, University of Craiova, 107 Decebal Boulevard, 200440 Craiova, Romania

P. Rotaru (✉)
Department of Physics, Faculty of Exact Sciences, University of Craiova, 13 AI Cuza Street, 200585 Craiova, Romania
e-mail: protaru@central.ucv.ro; petrerotaru@yahoo.com

S. Rizescu
Faculty of Mechanical Engineering, University of Craiova, 107 Calea Bucuresti Street, 200512 Craiova, Romania

N. G. Bîzdoacă
Faculty of Automation, Computers and Electronics, University of Craiova, 107 Decebal Boulevard, 200440 Craiova, Romania

designers, and companies recognized the potential to use the SME in engineering applications. As result, starting in the 1970s, commercial products began to appear [3, 7].

In the 1970s, more other alloys (Cu–Al–Ni, Cu–Zn–Al, Fe–Mn–Si, etc.) having properties of this kind were developed [6, 7].

Recently, Ti–Ni alloys have been extensively developed to check out some possible expansion of their application fields by adding new characteristics, shapes, and dimensions. Among them, some high temperature shape memory alloys have been developed: e.g., Ti–Ni–X (X = Au, Pd, Pt, Hf, and Zr) [9, 10].

The last 20 years witnessed a really dynamic evolution of these new materials in terms of studying their properties, improving, and diversifying their thinking technology. New and, sometimes, unexpected applying domains were found and new SMA-based systems (micro systems) were developed.

Applying domain for SMA-based actuators is really large and quite diversified: biomedical engineering, high precision engineering (positioning systems), robotics, automotive industry, electrotechnics, machine craft [11–19], etc.

More than one decade of authors' experience in the smart materials and structures research domain concerns not only material characterization and tests but also some design and simulation issues related to some SMA-powered original structures [5, 18–22]. Their work, carried out in the frame of some national or international specific projects, have been made on the material characterization (tests on SMAs) and on design, computation, and simulation of performances of such original structures as well. These studies have been focused especially on the robotics research domain. All this work has opened the way for the authors to identify some other potential application of SMAs in barrier structures. In this kind of respect, they have developed an experimental barrier structure, based on Ni–Ti SMA spring actuator, to analyze the operating mode, to insure the control of the active shape change of SMA spring.

Coverage on experimental model and operating mechanism

The way the experimental model was conceived is designed to comply with the study of the behavior of a small SMA-based barrier. As a qualitative assessment, we see no reason that a real barrier could work far different than a small one having the motion provided by a SMA spring.

In this model, the SMA spring is used to move the barrier arm, when it is activated. Their active shape change control can effectively increase the efficiency of such a barrier for several different regimes.

The experimental arrangement of the analyzed barrier which is powered by a Ni–TI SMA spring is shown in Fig. 1.

The arrangement description will concern the main components and that is only for a good understanding on how the structure does work.

The main element of this arrangement is the SMA Electric Piston (9), a linear actuator mechanism that shortens in length with great strength and speed when it is activated by carrying an electric direct current. An inside placed SMA spring makes all these possible. The SMA Electric Piston presented in Fig. 2, was purchased from the Mondo-tronics, Inc. [23].

The SMA spring presents two radically different forms or "phases" at the distinct temperatures M_f and A_f. At the "low" temperature (M_f), the SMA spring is extended, Fig. 2a, and can be stretched easily or deformed by a small force. However, when raised to the "high" temperature A_f, by carrying an electric direct current, the SMA spring changes to a much harder form. In this phase, Fig. 2b, it shortens in length, and exerts the force necessary to move the slider and to lift the barrier arm. The SMA Electric Piston used in our model can lift up to 4.5 N against gravity, yet the SMA Electric Piston weight is only 0.1 N.

If the SMA Electric Piston is overloaded (with any force bigger than 4.5 N), the steel made over-force spring gets into action, Fig. 2c. However, the maximum overload force the steel made over-load spring can support is 6.8 N.

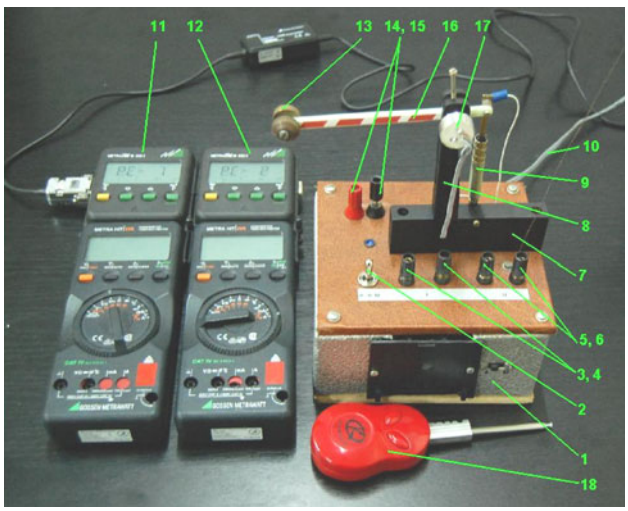

Fig. 1 Experimental arrangement of Ni–Ti SMA-based barrier: *1* internal power source box; *2* switch; *3, 4* connecting terminals for current measurement; *5, 6* connecting terminals for external power source; *7* seating base; *8* fixed support linked to seating base; *9* SMA Electric Piston; *10* plug-in table; *11* voltage channel of Data Acquisition System (DAS); *12* current channel of DAS; *13* metallic weight *G2* (external loading); *14, 15* connecting terminals for race transducer; *16* barrier arm; *17* race transducer; and *18* remote control

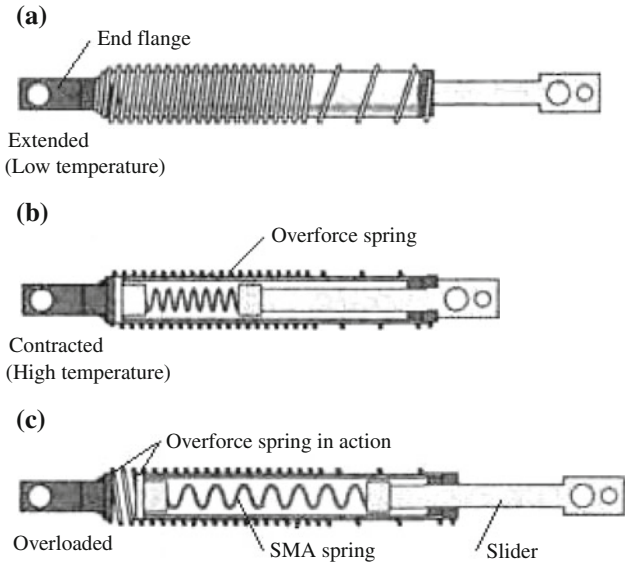

Fig. 2 SMA Electric Piston. © Mondo–tronics, Inc

Because the SMA Electric Piston activates by electric heating, the contraction time (and the barrier arm lifting time period, as well) varies significantly with the applied current; the higher the current, the faster the heating, and the faster the SMA contraction.

In the case of our model, the electric current for powering the SMA Electric Piston may come from two sources: an internal power source (Fig. 1, position 1) which insures a constant direct current, and an external power source, connected to the terminals (5) and (6), Fig. 1, which insure a variable direct current. In our study, for all the tests, the external power source was used.

Because the SMA spring material presents only the one-way shape memory effect, the recovering force is provided by the weight of the barrier arm and the weight $G2$ (Fig. 1, position 13).

For assessing the functional characteristics of this barrier, a Data Acquisition System (DAS) was used to collect data. The DAS was purchased from Gossen Metrawatt, and includes: race transducer-model 157 VISHAY (Fig. 1, position 17), two multi-meters METRAHit 29S (Fig. 1, positions 11 and 12), software METRAwin 10, and an interface BD232 via PC.

In order to achieve large motions in terms of angular displacements, the SMA actuator must be cleverly attached to the mechanism it operates. For our kinematic linkage, consisting in a moving arm barrier that pivots over a fixed revolute joint, the small linear displacements of a SMA spring actuator is converted into large angular motions by fixing the end flange (Fig. 2) of the actuator (SMA Electric Piston) and attaching the free end of the slider to the moving arm barrier close to the center of rotation of the revolute joint. This is very similar to how the biological muscles do move the links that make up the body. Of course, mechanical advantage is lost as the free end of the actuator is closer to the center of rotation [3].

Experimental

Analyzing the behavior of our barrier structure means to carry out the following experimental setup:

1. *Thermal analysis experiments*, to determine the transformation temperatures for the studied SMA spring during heating–cooling regime, under zero stress, and heat transfer of each process. Differential scanning calorimetry (DSC) method was used to determine the required parameters [2, 15, 17, 22, 24–31]. The specific heat is also determined during heating regime. The measurements were carried out on a horizontal diamond differential/thermo-gravimetric analyzer from PerkinElmer Instruments in dynamic air atmosphere, using aluminum crucible.
2. *Determination of the SMA spring working time periods* (time to start contracting t_{sc}, time to actuate t_a, relaxing time t_{rel}, and time to reset t_r) at different values of the activating electric current, when the stroke and the concentrated added on the barrier arm weight ($G2$) have constant values. The tests were made on the experimental model, using an external 40-V and 5-A stabilized power source. This source insures the possibility to get variable direct current.
3. The entire analysis was made using a Data Acquisition System with accommodative software and with a race transducer.
4. *Determination of the SMA spring lengths* using the real numerical values of the effective dimensions and dynamical parameters of the experimental model.

Results and discussion

Thermal analysis

It is well known that the SMAs exhibit a large temperature dependence on the material's shear modulus, which increases from low to high temperature. Therefore, as the temperature is increased the force exerted by a shape memory element increases dramatically [7, 32]. Consequently, the determination of the transformation temperatures is necessary to describe the dynamical response of the barrier structure.

To characterize the transformations of the SMA spring during the heating regime and cooling regime, corresponding to the lifting regime of the barrier arm and its

descent regime, respectively, it is necessary to establish all the four transformation temperatures: M_s, M_f, A_s, and A_f) [2, 15, 17, 22].

DSC test is a standard tool in the study of phase transformation. By measuring the relationship between power input/output and temperature change, it determines the phase transformation/temperature relation for a small specimen of the material [2].

The temperature range for the DSC measurement was from 15 to 100 °C under the controlled heating/cooling rate of 10 K min^{-1}, in a continuum dynamic air flow at 150 cm^3 min^{-1}. The SMA spring mass has constant value.

Figure 3 shows the detail of DSC curve for a 13.387 mg SMA spring material, during heating regime at 10 K min^{-1} heating stage.

The temperatures A_s and A_f, or M_s and M_f have been selected, where the DSC curve deviates from linearity.

Table 1 shows the experimentally obtained results from detailing the heating and cooling DSC curves in the above specified conditions.

During the period of time when the SMA spring acts on the barrier arm (meaning that the SMA spring does experience the heating regime), its specific heat values in dynamic air atmosphere were determined. Figures 4 and 5

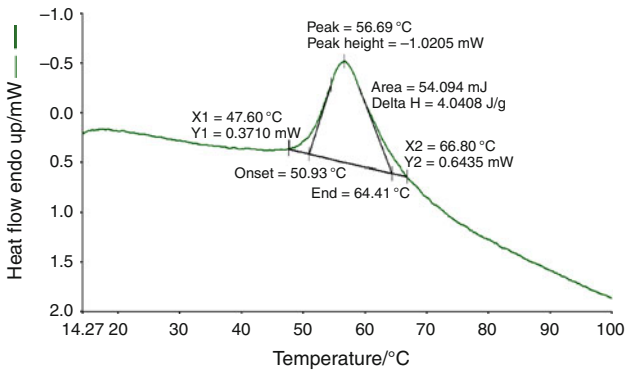

Fig. 3 Detail of DSC curve for phase transition (martensite to austenite) at heating of 10 K min^{-1}, for SMA spring material

Table 1 DSC parameters for SMA spring material

Phase transition	Thermal effect *endo/exo*	Transformation temperatures/°C	Temp. of the max. transformation rate/°C
Martensite to austenite (at heating)	Endothermic	$A_s = 47.60$ $A_f = 66.80$	56.69
Austenite to martensite (at cooling)	Exothermic	$M_s = 49.66$ $M_f = 27.10$	35.05

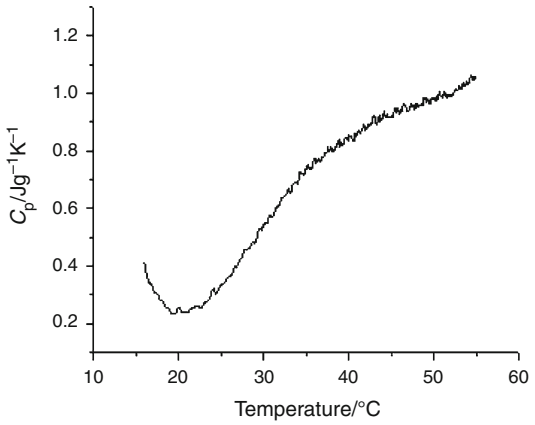

Fig. 4 Specific heat during heating regime at 2 K min^{-1} in martensitic status, for SMA spring material

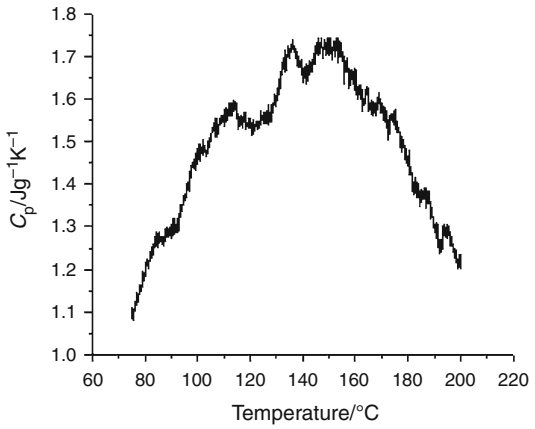

Fig. 5 Specific heat during heating regime at 2 K min^{-1} in austenitic status, for SMA spring material

are showing these values during heating regime in martensitic status and in austenitic status, respectively.

Specific heats were calculated using the formula:

$$c_p = \frac{1}{m}\frac{\delta Q}{dT} = \frac{1}{m}\frac{(\delta Q/dt)}{(dT/dt)} \quad (1)$$

Here the $(\delta Q/dt)$ is the heat flux given by the DSC curve, m is the sample mass, and $(dT/dt) = 10$ K $min^{-1} = 10/60$ K s^{-1} is the heating rate of the sample. T is the temperature and t is the time.

Uncertainty in determination of these temperatures is 0.1 K. This uncertainty induces an uncertainty in the calculation of c_p of 0.012–0.55 J g^{-1} K^{-1} in the temperature range of 21–57 °C, and of 0.059–0.085 J g^{-1} K^{-1} in the range 80–200 °C.

Some key issue here is that phase transitions are non-quasi-static processes. When it comes to discussion about the barrier arm lifting regime, what really concerns us is the martensitic phase into austenitic phase transition and continuing completely into austenitic phase as the heating

temperature goes up from A_f. The situation when $T > A_f$ is genuinely described in Fig. 5. Any thermal regime into this stabile phase can be described as a quasi-static regime in terms of heat exchange using a relation like this

$$\delta Q = mc_p(T)\,\mathrm{d}T \tag{2}$$

where physical issues have the following meanings: δQ is the elementary heat quantity exchanged by the spring material with its outside environment; m is the spring mass; and $\mathrm{d}T$ is the differential variation of thermodynamic temperature.

In this case, the relation (2) allows making assessments in terms of time, because the real heat transfer is made by electrical current trough its well-known Joule–Lenz effect:

$$Q = I^2 R\,t \tag{3}$$

with I, R and t are the direct activating current intensity, the electric resistance and the time of effectively heating through direct electric current up from A_f, respectively.

For an as much as possible exquisite control of the time resulting from equalization between relations (2) and (3) the $c_p(T)$ values given by Fig. 5 has to remain in the $[A_f, T_{final}]$ range, where we have $T_{final} = 110$ °C. This fact allows to maintain under certain control the relaxing time t_{rel}.

The same considerations could be made in case of quasi-static heating transfer regimes concerning the stable still martensitic phase and the corresponding to the also as much as possible exquisite control of the time to contract t_{sc}.

Determination of the SMA spring working time periods

This test was made to analyze the operating mode and to have control on active shape change of the SMA spring actuator.

The experiments concerning determination of the SMA spring working time periods (time to start contracting t_{sc}, time to actuate t_a, relaxing time t_{rel}, and time to reset t_r) were carried out at different values of the activating electric current, when the weight $G2$ and the stroke have constant values.

The race transducer converts the angular motion into electric voltage signal, as follows: 5 V corresponds to 340°. In our analysis, for all the tests, the value of the angular displacement (stroke) of barrier arm was 54.4°, which corresponds to 0.8 V voltage signal.

DAS made possible to put in evidence the displacement of the barrier arm as function of time for all activating currents.

As examples, in Fig. 6, the obtained results using a SMA activating direct current (I_a) of 2.7 A, for the weights $G2 = 0.28143$ N, is presented.

All results are detailed in the Table 2, where the parameters presented in this table mean as follows: t_{sc}, time to start contracting, or the necessary time from the start of current application to reach the temperature A_s; t_a, time to actuate, or the contraction time, or the necessary time for the arm to reach the angular displacement of 54.4°; and t_{rel}, relaxing time, or the necessary time for the SMA spring to cool from a temperature greater or at least equal to A_f to the temperature M_s. In all cases, the cooling process ended at 23.1 °C; t_r, time to reset, or the necessary time for the arm

Table 2 Times of work for the analyzed barrier corresponding to a complete cycle up-down

SMA activating direct current, I_a/A	Time to start contracting, t_{sc}/s	Time to actuate, t_a/s	Relaxing time, t_{rel}/s	Time to reset, t_r/s
1.76	24	51	14	63
1.92	20	25	14	60
2.22	14	14	13	61
2.7	10	8	12	59
3	6	6	11	59
3.8	3	4	11	57
4.2	3	3	11	56

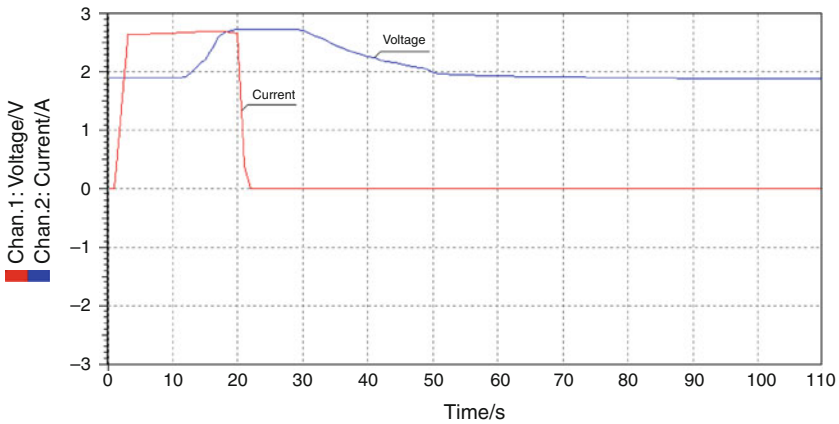

Fig. 6 Barrier arm displacement (stroke) and SMA active electric current time functions

to come back at its initial position. In this status, the SMA temperature is under M_f.

Watching results, it becomes obvious that because the SMA spring activates through electric heating, the contracting time varies in a quite significant range with the applied current; the higher the current, the faster the heating, and the faster the contraction, and so, the stroke of barrier arm considering the external weight as being constant.

The relaxing time values are not much different one from another and that is because the values of final heating temperatures ($T_{final} > A_f$) differ not too much, either, in each and every case.

We find ourselves able to choose a specific value for the current to obtain a desired pair of actuate-reset time periods.

Determination of the SMA spring lengths

In order to estimate the SMA spring lengths, the force F, developed by the Ni–Ti SMA spring was determined for static regime of the barrier structure. That means, dynamically, that the resulting moment of all forces with respect to O_0 (joining point between 16 and 8, Fig. 1) also takes zero value, so, we will have that:

$$kLF\cos q\cos q_1 - kLF\sin q\sin q_1 = m_1 gL\left(\frac{1}{2}-k\right)\cos q + m_2 gL(1-k)\cos q \quad (4)$$

This last relation leads us to the value of the force F, during a static regime:

$$F = \frac{k(\cos q_1 - tg\, q\sin q_1)}{m_1 g\left(\frac{1}{2}-k\right) + m_2 g(1-k)} \quad \text{with } k = \frac{AO_o}{AB} \quad (5)$$

In these relations, we made the following symbolic notations: L, length of the barrier arm; AO_0, distance from O_0 to the jointing point between the SMA actuator slider and the end of the barrier arm (A); q, angle between the barrier arm and the local horizontal that takes into consideration the regular trigonometric sense around the point O_0; q_1, angle between the longitudinal axis of the SMA actuator slider and the local vertical containing the end flange joint point that also takes into consideration the same trigonometric (positive) sense as q does; and m_1, mass of the barrier arm. The barrier arm is considered as being kind of homogenous and rigid; m_2, mass of the external concentrated weight $G2$ (Fig. 1, position 13).

With the following real values: $G_1 = 0.063$ N; $G_2 = 0.28143$ N; $L = 0.133$ m; $k = 0.1573373$; $q = 54°24'$; $\sin q = 0.8131$; $\cos q = 0.5821$; $\sin q_1 = 0.384$; and $\cos q_1 = 0.294$, the resulting actual value of the force $F \approx 3.87$ N.

We have neglected all loads related to the actuator design and that because they are very small indeed.

Concerning any SMA spring, bottom line is that its phase transitions during heating and cooling regimes and, correspondingly, its contracting and relaxing regimes are, in thermodynamic terms, non-quasi-static processes. In this respect, we have to add that it is really hard, at least for the time being, to issue any sort of thermodynamic-based constitutive equation having capabilities to directly connect the transversal shear modulus to thermodynamic temperature. That is why, in that follows, we shall calculate the SMA spring lengths only for the borders of stabile phases: $A_f = 66.80$ °C and $M_f = 27.10$ °C, values that are indicated in Table 1. For these temperatures, the values of shear modulus are, respectively, $G_h = 16{,}920$ and $G_l = 3{,}753$ MPa. The SMA spring must develop, at high temperature, the necessary force to lift the barrier arm by $S = 19$ mm on the direction of the SMA actuator slider axis corresponding to an angular experimentally measured displacement of the barrier arm of 54.4°. The value of this force, determined in the previous section, is $F = 3.87$ N.

The SMA spring data values Catalog (© Mondo-tronics, Inc.) are: wire diameter $d = 0.8$ mm; average diameter $D = 4$ mm, and number of active turns $n = 7$.

Using these values we can calculate [6, 7, 21, 23]:

– the spring rates at high and low temperature, K_h and K_l

$$K_h = \frac{G_h d^4}{8nD^3} = 1.9334 \text{ N/mm}, \quad (6)$$

$$K_l = \frac{G_l d^4}{8nD^3} = 0.4293 \text{ N/mm}; \quad (7)$$

– the spring deflections at high and low temperature, δ_h and δ_l

$$\delta_h = \frac{F}{K_h} = 2 \text{ mm}, \quad (8)$$

$$\delta_l = \delta_h + S = 21 \text{ mm}; \quad (9)$$

– the high and low temperature lengths, L_h and L_l.

The length of the spring when it is fully compressed at high temperature, L_f, is given by:

$$L_f = d \times (n+1) = 6.4 \text{ mm}$$

Under this condition, the following expression result for L_h and L_l:

$$L_h = L_f + \delta_h = 8.4 \text{ mm}, \quad (10)$$

$$L_l = L_h + S = 27.4 \text{ mm}. \quad (11)$$

Conclusions

The proposed barrier structure is kind of lightweight and has a simple configuration because it contains no hydraulic

fluids and compressor drive. SMA spring actuator offers efficiency in terms of energy, weight (it is always lighter), space and cost savings, and un-noisily operating, having, also, satisfactory life cycling requirements compared with a wide variety of products.

In normal functioning conditions, the SMA spring can perform many thousands of cycles in great reliability and repeatability, resulting in a long-life and huge efficiency SMA based barrier structure.

The active shape change control of the SMA spring can effectively increase the efficiency of a barrier at several different regimes.

Analyzing the experimental results, it turns out that our model behaves quite well in both cases of big and small activating currents. For a given barrier structure, choosing some certain values for external weight and activating current will be made at specific beneficiary request.

The experimental curves $c_p(T)$ shown in Figs. 4 and 5 were used in achieving a satisfactory control of t_{rel} and t_{sc}.

These new barrier structures may prove potential usefulness in: parking lots, toll gates, bridge barriers, apartment block access, toys, etc.

Acknowledgements This work was supported by CNCSIS–UEFISCSU (PNII–IDEI project 289/2008) and by the ANCS (PNII–CAPACITATI bilateral projects: 562/2010 with Turkey and 598/2010 with Korea).

References

1. Seung K, Byungkyu K. Design parametric study based fabrication and evaluation of in-pipe moving mechanism using shape memory alloy actuators. J Mech Sci. 2008;22:96–102.
2. Huang W. Shape memory alloys and their application to actuators for deployable structures. Ph.D. thesis, University of Cambridge; 1998.
3. Mavroidis C. Development of advanced actuators using shape memory alloys and electrorheological fluids. J Res Nondestr Eval. 2002;14:1–32.
4. Knowles G, Bird R, Birman V. Shape memory alloy springs used as reduced power/weight actuators. In: Proceedings of ASME 2004 international mechanical engineering congress and exposition, Anaheim, California, USA, November 13–9; 2004. p. 17–25.
5. Yang K, Gu CL. A compact and flexible actuator based on shape memory alloy springs. J Mech Eng Sci. 2008;222:1329–37.
6. Degeratu S, Bizdoaca NG. Shape memory alloys: fundamentals, design and applications. Craiova: Universitaria Press; 2003.
7. Waram TC. Actuator design using shape memory alloys. 1st ed. Hamilton: Ontario Press; 1993.
8. Funakubo H. Shape memory alloys. New York: Gordon and Breach Science; 1987.
9. Miyazaki S, Kim HY. Recent development of high temperature shape memory alloys for actuator applications. In: Proceedings of 2011 TMS annual meeting and exhibition, San Diego, California, USA, February 27–March 3; 2011.
10. Tello K, Cochran S, Neuchterlein I, Roman K, Drake D, et al. Characterization of new phases in the Ti–Pt system relevant to high temperature shape memory alloys. In: Proceedings of 2011 TMS annual meeting and exhibition, San Diego, California, USA, February 27–March 3; 2011.
11. Garner LJ, Wilson LN, Lagoudas DC. Development of a shape memory alloy actuated biomimetic vehicle. J Smart Struct Mater. 2000;9:673–83.
12. Strelec JK, Dimitris CL, Mohammad AK, Yen J. Design and implementation of a shape memory alloy actuated reconfigurable airfoil. J Intell Mater Syst Struct. 2003;14:257–73.
13. Paik JK, Hawkes E, Wood RJ. A novel low-profile shape memory alloy torsional actuator. J Smart Mater Struct. 2010;19. doi: 10.1088/0964-1726/19/12/125014.
14. Dolce M, Cardone D. Mechanical behavior of shape memory alloys for seismic applications 2: Austenitic NiTi wires subjected to tension. Int J Mech Sci. 2001;43:2657–77.
15. Chao-Chao R, Yu-Xing B, Hong-Mei W, Yu-Feng Z, Song LI. Phase transformation analysis of varied nickel–titanium orthodontic wires. J Chin Med. 2008;121(20):2060–4.
16. Wu Ming H, Schetky McDL. Industrial applications for shape memory alloys. In: Proceedings of the international conference on shape memory and superelastic technologies, Pacific Grove, California, USA; 2000. p. 171–82.
17. Nespoli A, Villa E, Besseghini S. Thermo-mechanical properties of snake-like NiTi wires and their use in miniature devices. J Therm Anal Calorim. 2011;. doi:10.1007/s10973-011-1324-0.
18. Bizdoaca NG, Degeratu S, Pana C, Vasile C. Fuzzy logic controller for hyperredundant shape memory alloy tendons actuated robot. In: Proceedings of the 7th international carpathian control conference, Ostrava Beskydy, Czech Republic; 2006. p. 53–6.
19. Bizdoaca NG, Degeratu S, Niculescu M, Pana D. Shape memory alloy based robotic ankle. In: Proceedings of 4th international carpathian control conference, Zakopane, Poland; 2004. p. 715–20.
20. Degeratu S, Rotaru P, Manolea Gh, Petrisor A, Bizdoaca NG. Visual Basic applications for shape memory elements design used in intelligent systems. In: Proceedings of 5th international conference on informatics in control, automation and robotics, Madeira, Portugal; 2008. p. 207–10.
21. Degeratu S, Bizdoaca NG, Manolea Gh, Diaconu I, Petrisor A, Degeratu V. Practical aspects regarding the design of intelligent systems using the shape memory alloy spring. In: Proceedings of Wseas international conference EMESEG, Heraclion, Crete, Greece; 2008. p. 226–31.
22. Degeratu S, Rotaru P, Manolea Gh, Manolea HO, Rotaru A. Thermal characteristics of Ni–Ti SMA (shape memory alloy) actuators. J Therm Anal Calorim. 2009;97(2):695–700.
23. Jameco electronics catalog. 2012;625. p. 61. ftp://ftp.jameco.com/Archive/PreviousCatalogs/624catalog.pdf.
24. Nespoli A, Besseghini S. A complete thermo-mechanical study of a NiTiCu shape memory alloy wire. J Therm Anal Calorim. 2011;103:821–6.
25. Petalis P, Makris N, Pasarras GC. Investigation of the phase transformation behaviour of constrained shape memory alloy wires. J Therm Anal Calorim. 2006;84:219–24.
26. Bouabdallah M, Cizeron G. Differential scanning calorimetry of transformation sequences during slow heating of Cu–Al–Ni shape memory alloys. J Therm Anal Calorim. 2002;68:951–6.
27. Auguet C, Isalgue A, Lovey FC, Pelegrina JL, Ruiz S, Torra V. Metastable effects on martensitic transformation in SMA. J Therm Anal Calorim. 2007;89:537–42.
28. Isalgue A, Torra V, Yawny A, Lovey FC. Metastable effects on martensitic transformation in SMA–part VI. The Clausius–Clapeyron relationship. J Therm Anal Calorim. 2008;91:8–991.
29. Sepulveda A, Munoz R, Lovey FC, Auguet C, Isalgue A, Torra V. Metastable effects on martensitic transformation in SMA. J Therm Anal Calorim. 2007;89:101–7.

30. Carreras G, Isalgue A, Torra V, Lovey FC, Soul H. Metastable effects on martensitic transformation in SMA–part V. Fatigue life and detailed hysteresis behavior in NiTi and Cu-based alloys. J Therm Anal Calorim. 2008;91:575–9.
31. Brailovski V, Prokoshkin S, Terriault P, Trochu F. Shape memory alloys: fundamentals, modeling and applications. Published by École de technologie supérieure (ETS), Université du Québec, Montreal. Part VI, chap. 19 Actuator applications; 2003. p. 731–54.
32. DeLaurentis KJ, Mavroidis C, Pfeiffer C. Development of a shape memory alloy actuated hand. In: Proceedings of the ACTUATOR 2000 conference, Bremen, Germany; 2000. p. 281–4.